



Density and Velocity Fluctuations of Alpha Particles in Magnetic Switchbacks

Michael D. McManus^{1,2}, Jaye Verniero³, Stuart D. Bale^{1,2}, Trevor A. Bowen², Davin E. Larson², Justin C. Kasper^{4,5}, Roberto Livi², Lorenzo Matteini⁶, Ali Rahmati², Orlando Romeo², Phyllis Whittlesey², and Thomas Woolley⁶

¹Physics Department, University of California, Berkeley, CA 94720-7300, USA; mdmcmanus@berkeley.edu

²Space Sciences Laboratory, University of California, Berkeley, CA 94720-7450, USA

³Heliophysics Science Division, NASA, Goddard Space Flight Center, Greenbelt, MD 20771, USA

⁴Climate and Space Sciences and Engineering, University of Michigan, Ann Arbor, MI 48109, USA

⁵Smithsonian Astrophysical Observatory, Cambridge, MA 02138 USA

⁶The Blackett Laboratory, Imperial College London, London, SW7 2AZ, UK

Received 2022 March 21; revised 2022 April 25; accepted 2022 April 27; published 2022 July 1

Abstract

Magnetic switchbacks, or sudden reversals in the magnetic field’s radial direction, are one of the more striking observations of the Parker Solar Probe (PSP) in its mission thus far. While their precise production mechanisms are still unknown, the two main theories are via interchange reconnection events and in situ generation. In this work, density and abundance variations of alpha particles are studied inside and outside individual switchbacks. We find no consistent compositional differences in the alpha particle abundance ratio, $n_{\alpha p}$, inside versus outside switchbacks, nor do we observe any signature when separating the switchbacks according to $V_{\alpha p}/V_{pw}$, the ratio of the alpha–proton differential speed to the wave phase speed (the speed at which the switchback is traveling). We argue that these measurements cannot be used to rule in favor of one production mechanism over the other, due to the distance between PSP and the postulated interchange reconnection events. In addition, we examine the 3D velocity fluctuations of protons and alpha particles within individual switchbacks. While switchbacks are always associated with increases in proton velocity, alpha velocities may be enhanced, unchanged, or decrease. This is due to the interplay between V_{pw} and $V_{\alpha p}$, with the Alfvénic motion of the alpha particles vanishing as the difference $|V_{pw} - V_{\alpha p}|$ decreases. We show how the Alfvénic motion of both the alphas and the protons through switchbacks can be understood as an approximately rigid arm rotation about the location of the wave frame, and illustrate that the wave frame can therefore be estimated using particle measurements alone, via sphere fitting.

Unified Astronomy Thesaurus concepts: Heliosphere (711); Solar wind (1534); Space plasmas (1544)

1. Introduction

One of the more striking results from the mission of the Parker Solar Probe (PSP; Fox et al. 2016) thus far is the ubiquity, in the near-Sun solar wind, of magnetic switchbacks (SBs) —large, sudden rotations of the magnetic field, accompanied by spikes in the radial solar wind velocity. While SBs have previously been observed both in the inner heliosphere, using Helios measurements (Borovsky 2016; Horbury et al. 2018), and at 1 au and beyond (Kahler et al. 1996; Neugebauer & Goldstein 2013), these recent PSP observations have sparked renewed interest in their nature and origins.

1.1. Properties

SBs are long, thin (Horbury et al. 2020; Laker et al. 2021), S-shaped (McManus et al. 2020) magnetic structures, most likely oriented along the magnetic field direction (Laker et al. 2021). They are mostly Alfvénic in nature, with a constant-magnitude $|\mathbf{B}|$ field corresponding to the condition of spherical polarization. The Alfvénic correlations between \mathbf{B} and \mathbf{v} mean that the field rotations of SBs are accompanied by large positive spikes in the proton velocity, regardless of the underlying polarity of the magnetic field (Matteini et al. 2014). They do not occur continuously, but rather appear in “patches” (Bale

et al. 2019; de Wit et al. 2020), separated by periods of quiet, steady flow and radial magnetic field. The proton core temperature appears unchanged within individual SBs (Woolley et al. 2020; Martinović et al. 2021), but the patches themselves appear to be hotter overall than the quiet interstitial periods (Bale et al. 2021; Woodham et al. 2021).

1.2. SB Formation Theories

The question of what mechanisms are responsible for SB generation is still an open one. Several ideas have been put forward, generally coming in two main flavors. The first involves generation via magnetic reconnection. Fisk & Kasper (2020) postulate that due to the large-scale equatorial circulation of the photospheric magnetic field, open magnetic field lines are dragged across closed loops at lower latitudes, causing interchange reconnection events that launch S-shaped kinks into the corona. Zank et al. (2020) describe a similar idea, but with the reconnection occurring significantly higher up in the corona, and launching fast magnetosonic-type modes both up and down the open field lines.

An alternative idea is that SBs naturally form in the solar wind as it expands and travels outward. Magnetic field fluctuations decay more slowly with radial distance R than the mean magnetic field does, resulting in the normalized amplitudes of Alfvénic fluctuations increasing as a function of R . This means that out of the bath of the initially small-amplitude, linear Alfvén waves that are known to be present at the base of the corona, the normalized fluctuation amplitudes grow as the plasma travels outward, until they eventually

become large enough to cause the field to switch back on itself. Mallet et al. (2021) develop an analytical model of such large-amplitude Alfvén waves in an expanding solar wind and make several testable predictions for the properties of the SBs produced, and similar results have been found via MHD simulations (Squire et al. 2020; Shoda et al. 2021). The in situ generation of SBs very naturally explains the observation that the SB filling fraction increases as a function of radius (Macneil et al. 2020; Mozer et al. 2020; Badman et al. 2021), something that is difficult to explain for theories involving a purely low coronal origin. It would also explain SB “patches” as corresponding to wind that has undergone greater expansion in transit; Bale et al. (2021) provide strong evidence that at least some of the patches observed by PSP so far are due to superradially expanded wind originating from the boundaries of supergranules at the solar surface.

However, recent analysis of Ulysses, Helios, and PSP data by Tenerani et al. (2021) suggests that the scaling of SB occurrence as a function of the radial distance R in fact depends on the size or duration of the SB, with shorter-duration SBs decaying with R and longer ones persisting. This, along with the nonuniform properties of SBs—which have a wide range of durations (de Wit et al. 2020), with some exhibiting compressibility, although most do not (Krasnoselskikh et al. 2020), and different types of discontinuity at the boundaries (Larosa et al. 2021), etc.—could be evidence that both types of generation mechanism are occurring, meaning that we are seeing a combination of short-duration SBs naturally decaying via processes like parametric decay within a few tens of solar radii (Tenerani et al. 2020), while in situ generation is replenishing the population of longer-duration SBs. At this stage, this is still speculative, and there are many open questions regarding the formation, evolution, and eventual decay of SBs.

For completeness, we mention that there are other potential SB generation mechanisms that are unrelated to the two just described. Ruffolo et al. (2020) suggest they may be associated with the onset of shear-driven turbulence at or above the Alfvén critical surface. Velocity shears between adjacent flux tubes can then potentially be large enough to trigger the onset of Kelvin–Helmholtz-type instabilities and their associated vorticity roll-ups, producing the large deflections in \mathbf{B} that we observe as SBs. Schwadron & McComas (2021) also postulate that SBs are produced by shear interactions between fast and slow streams above the Alfvén surface (when ram pressure becomes dominant), pointing out in particular that this should occur in the super-Parker spiral-type magnetic fields produced by footpoint motion across the leading edges of coronal holes.

In this paper, we focus on one small piece of the picture—the behavior of alpha particles inside as opposed to outside individual SBs, and whether or not this can help to distinguish between any potential generation mechanisms.

2. Methods

2.1. Data

For this study, we focus on PSP’s third and fourth encounters (E3 and E4) from 2019 August 27 to September 8, and from 2020 January 23 to February 3, respectively. We use data from the FIELDS magnetometers (Bale et al. 2016) for high-resolution magnetic field \mathbf{B} measurements, then downsample to match the particle measurement cadences as needed. 3D ion

velocity distribution function (VDF) measurements are taken from the SPAN-Ion electrostatic analyzer (Kasper et al. 2016; Livi et al. 2021), with proton and alpha count spectra produced at cadences of 7 s and 14 s, respectively. We fit a bi-Maxwellian to the proton channel spectra, to both the core and beam populations, with the proton beam constrained to lie along the magnetic field relative to the core velocity. The alpha channel contains a small (2%) contamination from the proton channel, which manifests as scaled-down proton core and beam VDFs in the alpha channel. This is accounted for by taking the previously fitted proton parameters and reducing the density down to fit the extraneous protons. An additional single bi-Maxwellian is then fit to the alpha part of the spectrum, and the core alpha particle VDF parameters are extracted. The $\sim 2\%$ scaling factor is a free parameter in the fit; it was checked that there was no energy or angle dependence in the contaminant protons, so that an overall scaling was sufficient. The uncertainties on the fitted alpha densities are approximately 10%.

We will on occasion require proton density measurements. For these, we use quasi-thermal noise (QTN) estimates derived from the extraction of the plasma line from the FIELDS RFS spectra (Romeo et al. 2021), and approximate $n_e = n_p + 2n_\alpha \approx n_p$, as the alpha abundance in PSP’s early encounters is very low (Woolley et al. 2021).

2.2. SBs

Our data set of SBs consists of 92 examples chosen by visual inspection from E3 and E4. Using the SPAN-Ion data as the source of our ion measurements means that we are constrained—by the alpha particle 14 s measurement cadence—to selecting relatively longer SBs, and so cannot use quite as large an event database as in some previous studies (Martinović et al. 2021). Following Martinović et al. (2021), we split each SB into five distinct regions: Leading Quiet (LQ), the relatively quiescent period immediately preceding the SB; Leading Transition (LT), the transition corresponding to the rotation of the magnetic field; Switchback Interior (SBI), the interior of the SB structure; Trailing Transition (TT), the second transition; and finally Trailing Quiet (TQ), the quiescent field immediately following the passing of the SB. In this work, we are mainly interested in comparing the quiescent “background” conditions to the SBIs, rather than the transition regions that represent the edges of the magnetic structure (and display a host of interesting physics, including signatures of reconnection (Froment et al. 2021) and wave activity (Agapitov et al. 2020; Krasnoselskikh et al. 2020)). Figure 1 shows a prototypical example SB, with the five regions indicated with the vertical dashed lines.

3. Results and Discussion

3.1. Density and Abundance Changes

The left plot in Figure 2 shows a histogram of the fractional change in alpha number density between the SBIs and their LQ regions, $(n_\alpha^{\text{SB}} - n_\alpha^{\text{LQ}})/n_\alpha^{\text{LQ}}$. While the spread in the fractional density changes is quite large, the mean (and median) of $\Delta n_\alpha/n_\alpha^{\text{LQ}}$ are both very close to zero (0.05 and 0.02, respectively). This is qualitatively very similar to the proton fractional density changes in SBs reported both in observations and simulations (see Figure 4 of Larosa et al. 2021 and Figure 10 of Shoda et al. 2021, respectively).

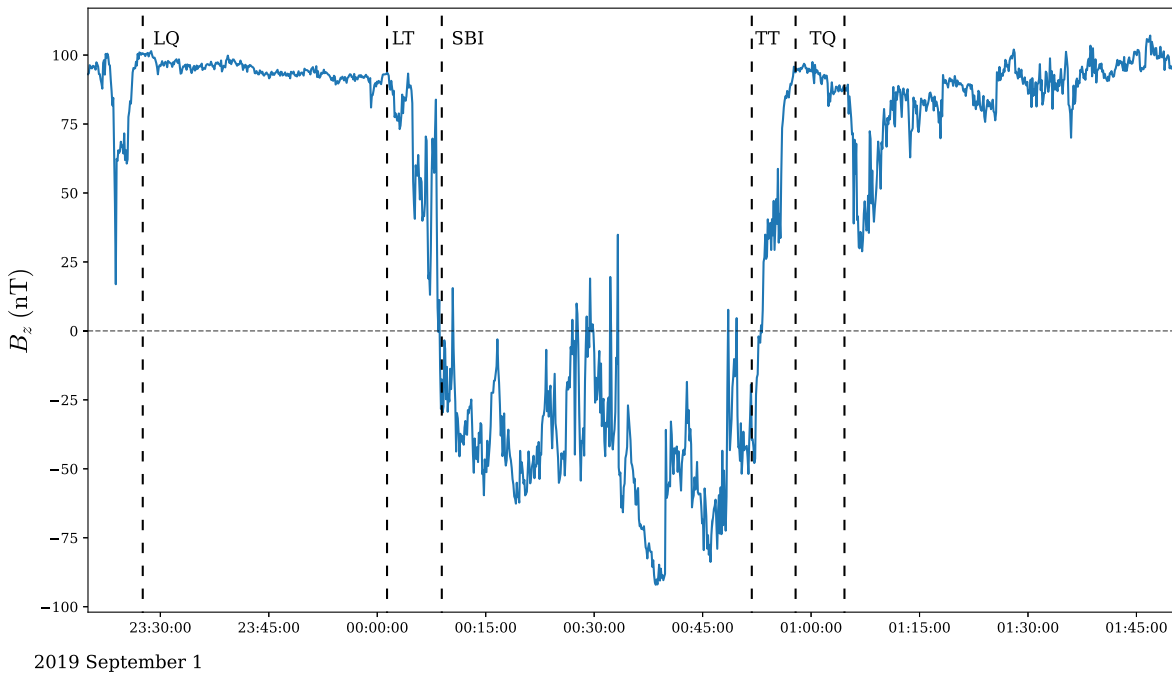


Figure 1. The z-component (in PSP spacecraft coordinates) of the magnetic field for a typical SB, showing the demarcation of the different regions: LQ, LT, SBI, TT, and TQ.

The histogram on the right in Figure 2 shows the change in alpha abundance $\Delta n_{\alpha p} = n_{\alpha}^{\text{SB}}/n_p^{\text{SB}} - n_{\alpha}^{\text{LQ}}/n_p^{\text{LQ}}$ between the same two regions (note that although one might have $\langle \Delta n_p \rangle \approx 0$ and $\langle \Delta n_{\alpha} \rangle \approx 0$, a priori they need not be statistically independent). For the proton densities, we do not use the SPAN-Ion measurements of n_p , but rather the estimates of n_p from the FIELDS QTN measurements, as detailed in Section 2. The large δV associated with SBs often moves the proton VDF significantly out of SPAN-Ion’s field of view, which results in a large (unphysical) proton density decrease, as measured by SPAN. While fitting does mitigate the problem somewhat, it is often not enough to completely eliminate these instrumental density decreases. Using SPAN-Ion measurements only would then appear to show large spikes in the alpha abundance inside SBs compared to outside them (not plotted here), which, as we have shown, is not the case. As we will explain in the next section, the alpha particle VDFs tend to move much less in velocity space during SBs, so the problem is much less significant, and any motion that does occur can be properly captured by the fitting routines. Again, while the spread in the right histogram of Figure 2 is relatively large, the distribution is clearly peaked at about $\Delta n_{\alpha p}/n_{\alpha p} \approx 0$. We interpret these two figures, then, as showing that there is no statistically significant change in either the alpha density or the alpha abundance inside SBs versus outside them.

The lack of a compositional signature difference between the SBI and LQ regions strongly suggests that we are measuring the same plasma inside versus outside them, in agreement with previous interpretations of SBs (Yamauchi et al. 2004; McManus et al. 2020; Woolley et al. 2020; Martinović et al. 2021). We would certainly expect SBs generated in situ not to display any compositional differences in the plasma inside the SB compared to that outside it. However, these observations do not rule out coronal origins of SBs. SBs generated by interchange reconnection events further down in the corona may very well be expected to display compositional differences

at the time when they are generated. This is because the properties of plasma confined in closed magnetic loops are known to change (relative to open field lines) over the confinement time, due to processes like gravitational settling and the first ionization potential effect (Rakowski & Laming 2012; Laming et al. 2019). However, the only way this would be measurable at PSP is if the alpha particles and the SB travel outward together at exactly the same speed from their point of origin, preserving the compositional signature difference. While it has long been generally understood that alpha particles *do* travel faster than the protons at approximately the local wave speed (Thieme et al. 1990; Steinberg et al. 1996; Matteini et al. 2015), giving rise to the phenomenon of alpha particle “surfing,” whereby alpha particles are less affected by Alfvénic fluctuations, we now show that this is not always the case, and that expecting a compositional signature to persist to PSP distances would require rather unphysical fine-tuning.

In Figure 3, we plot the change in alpha abundance $\Delta n_{\alpha p}$ versus the ratio of the alpha–proton drift speed to the wave speed, $V_{\alpha p}/V_W$. $V_{\alpha p}$ is calculated as $|V_{\alpha} - V_{pc}|$, where V_{α} and V_{pc} are the alpha and proton core velocities, respectively, and V_W is computed by taking the normal N-component of the equation

$$\delta V = \pm V_W \frac{\delta \mathbf{B}}{|\mathbf{B}|}, \quad (1)$$

which serves to define the wave speed (Goldstein et al. 1995). Plotting V_N versus $B_N/|\mathbf{B}|$ over the LQ region associated with each SB and taking the gradient of the line of best fit then yields an estimate of the local wave phase speed. (Note that Equation (1) is effectively an empirical measurement of the speed of the Alfvénic fluctuations—it is not yet fully understood why V_W is usually less than V_A in the solar wind (Goldstein et al. 1995; Neugebauer et al. 1996)).

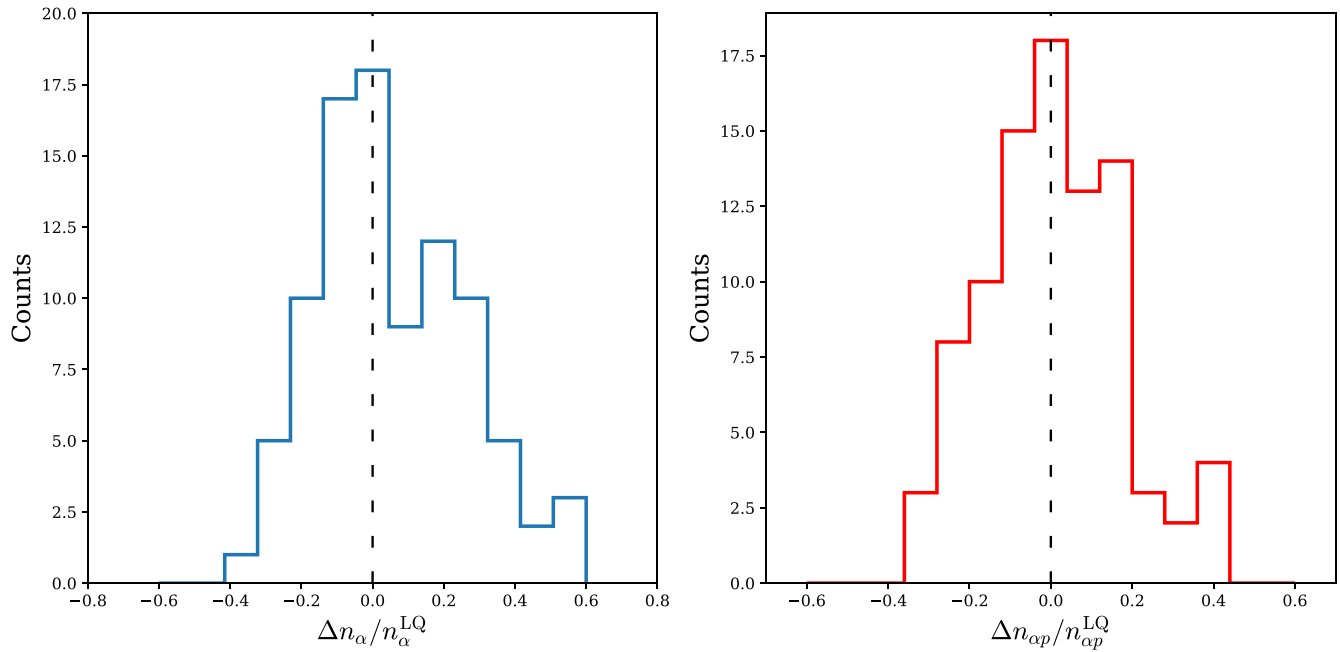


Figure 2. Histograms of the fractional change in alpha density (left) and alpha abundance (right) between SBIs and their LQ regions.

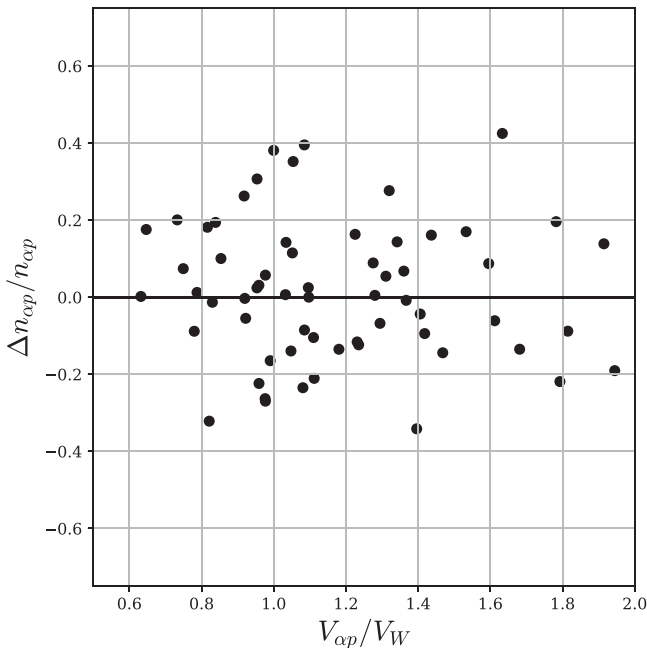


Figure 3. Scatter plot of the fractional change in alpha abundance in SBs vs. alpha-proton drift as a fraction of the local Alfvén wave phase speed. The distribution is symmetric, showing no strong dependence.

From Figure 3, we clearly see that the alpha particles do not always travel at the local wave speed; when considering short intervals such as these, there is a very wide range of $V_{\alpha p}/V_W$ values. There also does not appear to be any trend in $\Delta n_{\alpha p}$ with $V_{\alpha p}/V_W$. In particular, there is no signature around $V_{\alpha p}/V_W \approx 1$, where one might expect such a compositional signature to be, were it present when the SB was generated; the spread in points around $V_{\alpha p}/V_W \approx 1$ appears no different than the spread at other values. In retrospect, however, this is not too surprising, for two reasons. First, even in the model of Zank et al. (2020), where the interchange reconnection is occurring relatively high up (compared to the photospheric reconnection

models of Fisk & Kasper (2020) and Drake et al. (2021)), in coronal loops with scale height $\sim 6 R_{\odot}$, the local Alfvén speed is very high ($V_A \gtrsim 1000 \text{ km s}^{-1}$), and the alpha particles are not ever expected to drift at such high speeds ahead of the protons. Rather, the phenomenon of alpha particles surfing at the Alfvén speed is only expected to kick in at greater radial distances, once the Alfvén speed has decayed enough to be comparable to $V_{\alpha p}$ (and after which it may act as an instability threshold, preventing $V_{\alpha p} \gg V_A$ (Verscharen et al. 2013)). Thus, we would not expect $V_{\alpha p}/V_W \approx 1$ to be possible at the site of interchange reconnection, and the alphas would not be able to carry a compositional signature with the SB to be observed by PSP. Second, even if the alpha particles could leave the interchange reconnection event at the same speed as the SB, a PSP encounter with perihelion distance $\sim 30 R_{\odot}$ still represents a travel distance of several hundred Alfvén crossing times (using a typical SB length scale $l \sim 5 \times 10^4 \text{ km}$ (Tenerani et al. 2020; Laker et al. 2021)). Therefore, barring some rather unphysical fine-tuning, any compositional signature would have long since decayed away by the time the alpha particles reach PSP, and we would expect to observe something like Figure 3. In conclusion, then, our results are all consistent with in situ generation mechanisms of SBs, but cannot be used to rule out origin mechanisms occurring further down in the corona or at the surface of the Sun.

3.2. Alfvénic Motion of the Alphas

SBs are known to be highly Alfvénic and spherically polarized ($|\mathbf{B}| = \text{constant}$), and we therefore expect the particle motion to be spherically polarized, too. To see why, consider a particle at rest in a frame comoving with the Alfvén wave. The magnetic field, being Galilean-invariant, is still spherically polarized, and the wave being stationary means that energy is conserved in this frame (and that the electric field should almost vanish). A particle with the perturbed velocity $\delta \mathbf{v}$ relative to this frame must therefore trace out a sphere in velocity space in order to conserve energy. Boosting back into

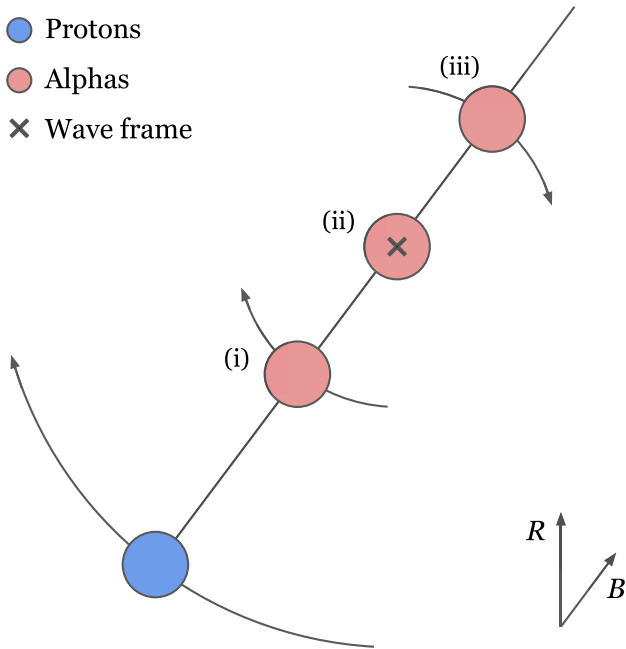


Figure 4. A cartoon showing the idealized expected alpha particle motion in velocity space during an SB in the three scenarios (i) $V_{\alpha p} < V_w$, (ii) $V_{\alpha p} \sim V_w$, and (iii) $V_{\alpha p} > V_w$, corresponding to the rows of Figure 5. R and B denote the radial and magnetic field directions, respectively.

the spacecraft frame, we infer that the observed motion should be spherically polarized, centered at the wave frame velocity, with a radius equal to the wave speed relative to whichever particle population we are considering. (For a more in-depth discussion of this, see Matteini et al. 2015.) With this picture in mind, one can potentially expect three different types of alpha particle motion, depending on the relative magnitudes of $V_{\alpha p}$ and V_{pw} ; these are sketched out in the cartoon in Figure 4. In scenario (i), we have $V_{\alpha p} < V_{pw}$, and would expect to observe the spherical polarization of both the protons and the alpha particles, with the alpha particles tracing out a sphere of smaller radius than the protons, approximately given by $V_{\alpha w} \approx V_{pw} - V_{\alpha p}$. In case (ii), the position of the alphas in velocity space roughly coincides with the wave frame, $V_{pw} \approx V_{\alpha p}$, and one would expect the protons to be spherically polarized, but the alphas to be roughly stationary. In case (iii), we have $V_{\alpha p} > V_{pw}$, and so we would again expect the protons and the alphas to be spherically polarized, but, importantly, the alphas should move in antiphase with the protons. This potential for alphas to move either in phase or in antiphase with the protons during the Alfvénic fluctuations, depending on the relative values of $V_{\alpha p}$ and V_{pw} , was first pointed out by Goldstein et al. (1995), using Ulysses data. Understanding this in terms of the spherical motion of each species in velocity space is exactly the model laid out in Matteini et al. (2015), the only difference here is that the cadence and quality of the SPAN-Ion measurements allow us to distinguish between the three cases over short timescales, and directly observe and measure the spherical polarization of the alphas.

In each row of Figure 5, we show an example SB, illustrating the three main types of alpha particle motion just described. The left column shows the 3D proton and alpha velocity measurements (in blue and red, respectively), in instrument coordinates. In all three cases, the proton motion (in blue) is spherically polarized, as expected. Regarded as single, large-

amplitude, low-frequency Alfvén waves, these SBs are not just spherically polarized, but to a good approximation arc-polarized as well (Fisk & Kasper 2020), as first theoretically predicted by Barnes & Hollweg (1974) and observed many times in the solar wind since (Lichtenstein & Sonett 1980; Tsurutani et al. 1994; Riley et al. 1996). Their maximum and intermediate principal component axes define a plane that is almost constant through the SB interval, and the tip of the \mathbf{B} field roughly traces out an arc on the sphere of $|\mathbf{B}| = \text{constant}$. If \mathbf{e}_1 , \mathbf{e}_2 , and \mathbf{e}_3 are the orthonormal principal components of the magnetic field measurements \mathbf{B}_i for a single SB interval with eigenvalues $\lambda_1 \lesssim \lambda_2 \ll \lambda_3$, we can project the measurements onto the plane defined by \mathbf{e}_2 and \mathbf{e}_3 , which should be the plane in which they appear most circular; this is shown in the third column of Figure 5. The fluctuations being Alfvénic means that we can project the velocity measurements onto the same plane; this is plotted in the second column of Figure 5.

From the middle plot of the first SB example (taken from 2019-08-30/22:50:25 to 2019-08-30/23:12:47), we can see that the alpha particle velocities in red are spherically polarized as well, albeit with smaller amplitude—they move on the surface of a smaller sphere. To a good approximation, the alpha and proton velocities both subtend the same angle θ that the magnetic field does, and appear to be rotating about a similar point in velocity space. The yellow circle represents the start of the entire SB interval, and the yellow triangle represents the point of the maximum \mathbf{B} field deflection during the SB. From these, we can see that the protons and alphas are moving in phase with each other. This corresponds to scenario (i), $V_{\alpha p} < V_{pw}$, in Figure 4. Circles of best fit to the proton and alpha motions are overlaid in blue and red, respectively, their centers marked with crosses. The proximity of the centers of the alpha and proton circles shows good agreement between these two components of the wave frame velocity. The third component can be estimated by calculating the $(\mathbf{e}_2, \mathbf{e}_3)$ plane that minimizes the least square distance to the measured velocities for each species separately (this is then the plane of arc polarization). For protons, the sphere center is $\mathbf{v}_{pw} = (-543, 147, 16) \text{ km s}^{-1}$, and for the alphas it is $\mathbf{v}_{\alpha w} = (-547, 152, 28) \text{ km s}^{-1}$ (in instrument coordinates), showing very good agreement in all three components. Because the alpha fits are independent of the proton fits (they are not constrained to lie along the magnetic field relative to the proton VDFs), fitting spheres in this way represents two independent estimates of the wave frame velocity.

Using Equation (1) for the LQ region of this SB, we estimate the local alpha and proton wave phase speeds as $V_{pw} \approx 149 \text{ km s}^{-1}$ and $V_{\alpha w} \approx 45 \text{ km s}^{-1}$, respectively. This is in excellent agreement with the radii of the spheres of best fit in column 2, which have radii of 143 and 44 km s^{-1} , respectively. With $V_{\alpha p} \approx 114 \text{ km s}^{-1}$ in the LQ region, we also have $V_{\alpha p} < V_{pw}$ and $V_{\alpha p} + V_{\alpha w} \approx V_{pw}$, as expected. Comparing to the measured Alfvén speed $V_A \approx 147 \text{ km s}^{-1}$ for this SB, we see that the proton phase speed and the Alfvén speed are almost equal, $V_{pw} \approx 1.01 V_A$. In the time series of the particle velocities for SBs like this, the large spikes in proton velocity would also be seen in the alphas, albeit smaller in magnitude.

In the second example SB (middle row; taken from 2019-08-29/21:08:04 to 2019-08-29/21:20:46), the proton velocities are still spherically polarized, but the alphas are not—they appear relatively stationary in velocity space through the SB and do not trace out an arc (the yellow markers of initial and

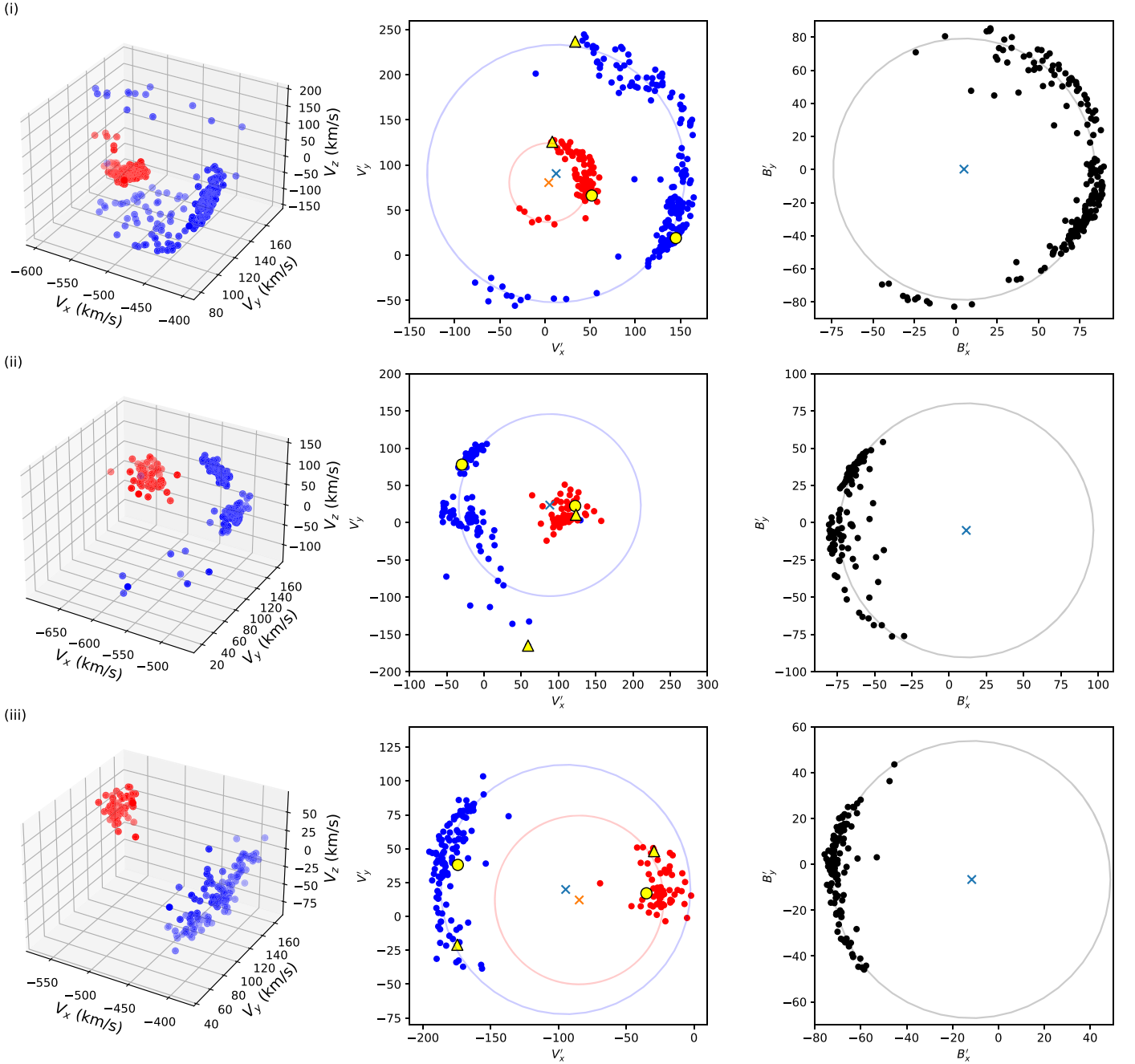


Figure 5. Three example SBs showing the different types of alpha particle Alfvénic motion. The first column shows the 3D proton and alpha velocity measurements in instrument coordinates, in blue and red, respectively, through the SB. The middle column shows these particle velocities projected onto the minimum variance magnetic field plane. The yellow circles indicate the start of the SB interval, while the yellow triangles indicate the point of maximum deflection during the SB. The third column shows the magnetic field measurements projected onto the same plane, with circles of best fit in gray (the blue crosses mark the circles’ centers).

maximum \mathbf{B} deflection lie almost on top of each other). This corresponds to scenario (ii) in Figure 4, where $V_{\text{cw}} \approx 0$, and for the LQ interval preceding this SB, we have $V_{\text{cp}} \approx 158 \text{ km s}^{-1}$, $V_{\text{pw}} \approx 162 \text{ km s}^{-1}$, and $V_{\text{cw}} \approx 6 \text{ km s}^{-1}$, with $V_A \approx 161 \text{ km s}^{-1}$, so that $V_{\text{pw}} \approx 1.01 V_A$. The alphas are therefore roughly comoving with the wave, and their location in velocity space serves as an estimate of the wave frame. The center of the proton circle of best fit in blue lies reasonably close to the alpha velocities, but we note that there is a fair amount of scatter in the proton measurements for this SB.

Finally, in the third example SB in the bottom row (from 2019-08-29/08:37:52 to 2019-08-29/08:51:09), the alphas are

again spherically polarized, but moving in antiphase with the protons, as can be seen by the relative locations of the points of maximum SB deflection (the yellow triangles). This corresponds to scenario (iii) in Figure 4. For this LQ region, we have $V_{\text{cp}} \approx 167 \text{ km s}^{-1}$, $V_{\text{pw}} \approx 101 \text{ km s}^{-1}$, and $V_{\text{cw}} \approx -26 \text{ km s}^{-1}$, with $V_A \approx 105 \text{ km s}^{-1}$, so that $V_{\text{pw}} \approx 0.96 V_A$. The quantitative agreement is not quite as good as before, but qualitatively $V_{\text{cp}} > V_{\text{pw}}$, and V_{cw} and V_{pw} have opposite signs, as expected. For SBs such as these, a time series of the particle velocities would see spikes in proton velocity coinciding with dips in alpha velocity. We note that this antiphase motion would also be expected to be observed in proton beams, since

Table 1
Wave Speeds Determined by Sphere Fitting versus V_{DHT}

SB	v_{pw} (km s^{-1})	V_{DHT} (km s^{-1})
(i)	(−543, 147, 16)	(−548, 116, 9)
(ii)	(−598, 155, 33)	(−614, 152, 12)
(iii)	(−483, 128, 1)	(−473, 123, 9)

they typically travel at or slightly above the Alfvén speed relative to the core (Alterman et al. 2018).

3.3. Relation to the de Hoffman–Teller Frame

Finally, for completeness, we compare the wave frames determined using the methods described above with the direct computation of the de Hoffman–Teller (DHT) frame. First introduced by de Hoffmann & Teller (1950) in the context of MHD shocks, this is defined as the frame in which the plasma’s electric field vanishes, and is usually computed by finding the velocity \mathbf{V} that minimizes the quantity (Khrabrov & Sonnerup 1998)

$$D(\mathbf{V}) = \frac{1}{M} \sum_{m=1}^M |(\mathbf{v}^{(m)} - \mathbf{V}) \times \mathbf{B}^{(m)}|^2, \quad (2)$$

where $\mathbf{v}^{(m)}$ and $\mathbf{B}^{(m)}$ denote the velocity and magnetic field values over a series of measurements indexed by $m = 1, \dots, M$. By definition, we expect the DHT frame and the wave frames computed above to be one and the same. To see geometrically why this is so for the SBs being considered here, consider the ideal case of a perfectly spherically polarized Alfvén wave. The minimum value of $D(\mathbf{V}) = 0$ will be achieved only if each term in Equation (2) vanishes, which requires \mathbf{V}_{DHT} to lie on the line through $\mathbf{v}^{(m)}$ parallel to $\mathbf{B}^{(m)}$, for each measurement m . The point that uniquely satisfies this is the center of the sphere in velocity space (as it is the point of intersection of each of these lines through $\mathbf{v}^{(m)}$). Thus, regarding SBs as essentially single, large-amplitude, spherically polarized Alfvén waves, we expect \mathbf{V}_{DHT} and v_{pw} to agree to good approximation, and this is indeed the case for our three example SBs, as summarized in Table 1.

4. Conclusions

In this work, the density and abundance variations of alpha particles were examined in a database of 92 SBs from PSP encounters E3 and E4. No consistent compositional signature difference was observed in the alpha abundance $n_{\alpha p}$ inside the SBs versus outside them, suggesting that PSP is measuring the same plasma in both cases, in agreement with previous interpretations of SBs (Yamauchi et al. 2004; Woolley et al. 2020; Martinović et al. 2021). We argued that even if SBs are the results of interchange reconnection events lower down in the corona, compositional signatures are not likely to exist and be measurable at PSP for two reasons: (1) the local Alfvén speed at the postulated interchange reconnection sites is very high and most likely precludes alphas being able to travel with the SBs that are launched upward along the field lines (thus preventing compositional information being carried with the SB); and (2) even if the alphas are able to travel with the SB, a small difference between $V_{\alpha p}$ and V_{pw} would result in a

compositional signature to have long decayed away due to the distance (in Alfvén crossing times) to PSP’s perihelia. Thus, our observation of there being no dependence of $\Delta n_{\alpha p}$ on $V_{\alpha p}/V_{pw}$ is to be expected, and it does not help to distinguish between in situ generation and interchange reconnection as potential SB formation mechanisms.

In addition, we examined the 3D nature of the velocity fluctuations of both protons and alphas within individual SBs. We observed the spherical polarization of both the proton and alpha velocities, which can be understood as a consequence of energy conservation in the wave frame. Three example SBs showed the alphas moving in phase, being stationary relative to, and moving in antiphase with the protons. This corresponds to the three cases $V_{\alpha p} < V_{pw}$, $V_{\alpha p} \approx V_{pw}$, and $V_{\alpha p} > V_{pw}$. Thus, while SBs are always associated with spikes in proton velocity, alpha velocities may be enhanced, unchanged, or decrease, depending on the relative values of $V_{\alpha p}$ and V_{pw} . For the case $V_{\alpha p} < V_{pw}$, where the alphas move in phase on a sphere of smaller radius than the protons, the centers of the proton and alpha velocity spheres were in excellent agreement, illustrating how one can make two independent particle measurements to uniquely identify the wave frame. One can in principle use these methods to estimate the wave frame over short timescales, using purely particle measurements, and we showed that this agreed well with the usual method of computing the DHT frame via the minimization of the motional electric field, $\mathbf{E} = -\mathbf{v} \times \mathbf{B}$. Intuitively then, the Alfvénic motion of both the alphas and the protons through SBs can be understood as an approximately rigid arm rotation about the location of the wave frame in velocity space, as illustrated in Figure 4 and discussed in Matteini et al. (2014, 2015), with the length of the lever arms to a good approximation being given by V_{pw} and $V_{\alpha w}$ for protons and alphas, respectively.

ORCID iDs

Michael D. McManus  <https://orcid.org/0000-0001-6077-4145>
 Jaye Verniero  <https://orcid.org/0000-0003-1138-652X>
 Stuart D. Bale  <https://orcid.org/0000-0002-1989-3596>
 Trevor A. Bowen  <https://orcid.org/0000-0002-4625-3332>
 Davin E. Larson  <https://orcid.org/0000-0001-5030-6030>
 Justin C. Kasper  <https://orcid.org/0000-0002-7077-930X>
 Roberto Livi  <https://orcid.org/0000-0002-0396-0547>
 Lorenzo Matteini  <https://orcid.org/0000-0002-6276-7771>
 Ali Rahmati  <https://orcid.org/0000-0003-0519-6498>
 Orlando Romeo  <https://orcid.org/0000-0002-4559-2199>
 Phyllis Whittlesey  <https://orcid.org/0000-0002-7287-5098>
 Thomas Woolley  <https://orcid.org/0000-0002-9202-619X>

References

- Agapitov, O., de Wit, T. D., Mozer, F., et al. 2020, *ApJL*, 891, L20
 Alterman, B., Kasper, J. C., Stevens, M. L., & Koval, A. 2018, *ApJ*, 864, 112
 Badman, S. T., Bale, S. D., Rouillard, A. P., et al. 2021, *A&A*, 650, A18
 Bale, S., Goetz, K., Harvey, P., et al. 2016, *SSRv*, 204, 49
 Bale, S., Badman, S., Bonnell, J., et al. 2019, *Natur*, 576, 237
 Bale, S., Horbury, T., Velli, M., et al. 2021, *ApJ*, 923, 174
 Barnes, A., & Hollweg, J. V. 1974, *JGR*, 79, 2302
 Borovsky, J. E. 2016, *JGRA*, 121, 5055
 De Hoffmann, F., & Teller, E. 1950, *PhRv*, 80, 692
 de Wit, T. D., Krasnoselskikh, V. V., Bale, S. D., et al. 2020, *ApJS*, 246, 39
 Drake, J., Agapitov, O., Swisdak, M., et al. 2021, *A&A*, 650, A2
 Fisk, L., & Kasper, J. 2020, *ApJL*, 894, L4
 Fox, N., Velli, M., Bale, S., et al. 2016, *SSRv*, 204, 7
 Froment, C., Krasnoselskikh, V., de Wit, T. D., et al. 2021, *A&A*, 650, A5
 Goldstein, B., Neugebauer, M., & Smith, E. 1995, *GeoRL*, 22, 3389

- Horbury, T., Matteini, L., & Stansby, D. 2018, *MNRAS*, **478**, 1980
- Horbury, T. S., Woolley, T., Laker, R., et al. 2020, *ApJS*, **246**, 45
- Kahler, S., Crocker, N., & Gosling, J. 1996, *JGRA*, **101**, 24373
- Kasper, J. C., Abiad, R., Austin, G., et al. 2016, *SSRv*, **204**, 131
- Khrabrov, A. V., & Sonnerup, B. U. 1998, Analysis methods for multi-spacecraft data, Vol. 1 (The Netherlands: ESA Publications Division), 221
- Krasnoselskikh, V., Larosa, A., Agapitov, O., et al. 2020, *ApJ*, **893**, 93
- Laker, R., Horbury, T. S., Bale, S. D., et al. 2021, *A&A*, **650**, A1
- Laming, J. M., Vourlidas, A., Korendyke, C., et al. 2019, *ApJ*, **879**, 124
- Larosa, A., Krasnoselskikh, V., Dudok de Wit, T., et al. 2021, *A&A*, **650**, A3
- Lichtenstein, B., & Sonett, C. 1980, *GeoRL*, **7**, 189
- Livi, R., Larson, D. E., Kasper, J. C., et al. 2021, *E&SS*, submitted
- Macneil, A. R., Owens, M. J., Wicks, R. T., et al. 2020, *MNRAS*, **494**, 3642
- Mallet, A., Squire, J., Chandran, B. D., Bowen, T., & Bale, S. D. 2021, *ApJ*, **918**, 62
- Martinović, M. M., Klein, K. G., Huang, J., et al. 2021, *ApJ*, **912**, 28
- Matteini, L., Horbury, T., Pantellini, F., Velli, M., & Schwartz, S. 2015, *ApJ*, **802**, 11
- Matteini, L., Horbury, T. S., Neugebauer, M., & Goldstein, B. E. 2014, *GeoRL*, **41**, 259
- McManus, M. D., Bowen, T. A., Mallet, A., et al. 2020, *ApJS*, **246**, 67
- Mozer, F., Agapitov, O., Bale, S., et al. 2020, *ApJS*, **246**, 68
- Neugebauer, M., Goldstein, B., Smith, E., & Feldman, W. 1996, *JGRA*, **101**, 17047
- Neugebauer, M., & Goldstein, B. E. 2013, in Proc. of the 13th Int. Solar Wind Conf., AIP Conf. Proc. 1539 (College Park, MD: AIP), 46
- Rakowski, C. E., & Laming, J. M. 2012, *ApJ*, **754**, 65
- Riley, P., Sonett, C., Tsurutani, B., et al. 1996, *JGRA*, **101**, 19987
- Romeo, O., Larson, D. E., Whittlesey, P. L., et al. 2021, in AGU Fall Meeting 2021 (Washington, DC: AGU)
- Ruffolo, D., Matthaeus, W. H., Chhiber, R., et al. 2020, *ApJ*, **902**, 94
- Schwadron, N., & McComas, D. 2021, *ApJ*, **909**, 95
- Shoda, M., Chandran, B. D., & Cranmer, S. R. 2021, *ApJ*, **915**, 52
- Squire, J., Chandran, B. D., & Meyrand, R. 2020, *ApJL*, **891**, L2
- Steinberg, J., Lazarus, A., Ogilvie, K., Lepping, R., & Byrnes, J. 1996, *GeoRL*, **23**, 1183
- Tenerani, A., Sioulas, N., Matteini, L., et al. 2021, *ApJL*, **919**, L31
- Tenerani, A., Velli, M., Matteini, L., et al. 2020, *ApJS*, **246**, 32
- Thieme, K., Marsch, E., & Schwenn, R. 1990, *AnGeo*, **8**, 713
- Tsurutani, B., Ho, C., Smith, E., et al. 1994, *GeoRL*, **21**, 2267
- Verscharen, D., Bourouaine, S., & Chandran, B. D. 2013, *ApJ*, **773**, 163
- Woodham, L., Horbury, T., Matteini, L., et al. 2021, *A&A*, **650**, L1
- Woolley, T., Matteini, L., Horbury, T. S., et al. 2020, *MNRAS*, **498**, 5524
- Woolley, T., Matteini, L., McManus, M. D., et al. 2021, *MNRAS*, **508**, 236
- Yamauchi, Y., Suess, S. T., Steinberg, J. T., & Sakurai, T. 2004, *JGRA*, **109**, A03104
- Zank, G., Nakanotani, M., Zhao, L.-L., Adhikari, L., & Kasper, J. 2020, *ApJ*, **903**, 1